and becomes oxidized to its radical form, thereby generating the active RRB2.[49] However, in the case of 1, we have been unable to intercept the putative peroxo intermediate with appropriate substrates.

Acknowledgment. This work was supported by funds from the National Institutes of Health (Grant GM-38767) and the University of Minnesota Graduate School. We thank Dr. Carlos Juarez-Garcia and Professor Eckard Münck for providing the Mössbauer spectrum of 1 and Dr. Ho G. Jang for his valuable assistance with the magnetic susceptibility experiments and their analysis.

Supplementary Material Available: Tables listing fractional atomic coordinates, thermal factors, and all bond lengths and angles for 1 and Figure S1, showing the Mössbauer spectrum of 1 and its theoretical fit (18 pages). Ordering information is given on any current masthead page.

The Intercalation Reaction of Pyridine with Manganese Thiophosphate, $MnPS_3$

Pattayil Alias Joy and Sukumaran Vasudevan*

Contribution from the Department of Inorganic and Physical Chemistry, Indian Institute of Science, Bangalore-560012, India. *Received March 27, 1992*

Abstract: The intercalation of pyridine in the layered manganese thiophosphate, $MnPS_3$, has been examined in detail by a variety of techniques. The reaction is interesting since none of the anticipated changes in optical and electrical properties associated with intercalation of electron donating molecules is observed. The only notable change in the properties of the host lattice is in the nature of the low-temperature magnetic ordering; while $MnPS_3$ orders antiferromagnetically below 78 K, the intercalated compound shows weak ferromagnetism probably due to a canted spin structure. Vibrational spectra clearly show that the intercalated species are pyridinium ions solvated by neutral pyridine molecules. The corresponding reduced sites of the host lattice, however, were never observed. The molecules in the solvation shell are exchangeable. Although the reaction appears to be topotactic and reversible, from XRD, a more detailed analysis of the products of deintercalation reveal that it is not so. The intercalation proceeds by an ion exchange/intercalation mechanism wherein the intercalated species are pyridinium ions solvated by neutral molecules with charge neutrality being preserved not by electron transfer but by a loss of Mn^{2+} ions from the lattice. The experimental evidence leading to this conclusion is discussed and it is shown that this model can account satisfactorily for the observed changes (or lack of it) in the optical, electrical, vibrational, and magnetic properties.

I. Introduction

The intercalation reaction in layered lattices provides a unique route to the study of host-guest interactions in various environments.[1,2] In this paper we report a detailed investigation of the intercalation in the layered transition metal thiophosphates,[3] MPS_3, using the Lewis base pyridine as a probe guest species. What makes the transition metal thiophosphates interesting is that although they bear a strong structural resemblance (Figure 1) to the well-studied transition metal dichalcogenides,[4,5] MX_2, and like them can intercalate a wide variety of electron donating molecules[6] within the van der Waals gap the nature of metal-ligand interactions is much more ionic[7] as compared to the transition metal dichalcogenides. This provides a unique opportunity to contrast the behavior and properties of the same guest molecule intercalated in structurally similar lattices possessing widely different types of bonding.

In light of numerous experimental investigations,[7,8] it is generally agreed that MPS_3 compounds are best viewed as salts of the thiophosphate anion, $M_2^{2+}(P_2S_6)^{4-}$, rather than as metal phosphorus sulfides. The M^{2+} ions are in the high spin state, and the compounds are magnetic undergoing a low-temperature magnetic transition to an antiferromagnetic state.[9] In contrast the M-X bonds in the transition metal dichalcogenides are much more covalent, and a much better description of the d electrons is the band model.[5]

The intercalation behavior of the transition metal dichalcogenides is well documented in the literature.[1,2,10] Much of the spectacular change in conductivity,[11] optical properties,[12] and superconductivity[13] can be understood in terms of a simple charge transfer model[11] in which electrons are transferred from the guest species to the host lattice. In the case of pyridine intercalation in NbS_2, TaS_2, etc., however, the orientation of pyridine molecules in their van der Waals gap[14,15] disallows any direct interaction between the nitrogen lone pair and the host lattice. The existence of pyridinium ions as an intercalated species has led to the postulation of a different mechanism, the Schöllhorn

(1) Levy, F., Ed. *Intercalated Layered Materials*; D. Riedel: Dordrecht, 1979.
(2) Whittingham, M. S.; Jacobson, A. J., Eds. *Intercalation Chemistry*; Academic: New York, 1982.
(3) Klingen, W.; Ott, R.; Hahn, H. *Z. Anorg. Allg. Chem.* **1973**, *396*, 271-278.
(4) Levy, F., Ed. *Crystallography and Crystal Chemistry of Materials with Layered Structures*; D. Riedel: Dordrecht, 1976.
(5) Wilson, J. A.; Yoffe, A. D. *Adv. Phys.* **1969**, *73*, 193-335.
(6) Brec, R. *Solid State Ionics* **1986**, *22*, 3-30. Johnson, J. W. In ref 2, Chapter 8, pp 267-283.
(7) Joy, P. A. Ph.D. Thesis 1990, IISc, Bangalore.
(8) Piacentini, M.; Grasso, V.; Santangelo, S.; Fanfoni, M.; Modesti, S.; Savoir, A. *Solid State Commun.* **1984**, *51*, 467-471. Ohno, Y.; Hirama, K. *J. Solid State Chem.* **1986**, *63*, 258-266. Grasso, V.; Neri, F.; Santangelo, S.; Silipigni, L.; Piacentini, M. *Phys. Rev.* **1988**, B37, 4419-4424.
(9) Le Flem, G.; Brec, R.; Ouvrard, G.; Louisy, A.; Segransan, P. *J. Phys. Chem. Solids* **1982**, *43*, 455-461.
(10) Whittingham, M. S.; Dines, M. B. *Surv. Prog. Chem.* **1980**, *9*, 55-57. Gamble, F. R.; Geballe, T. H. *Treatise Solid State Chem.* **1980**, *3*, 89-166. *Proc. Int. Conf. Layered Materials and Intercalates, Physica* **1980**, *99B*. Whittingham, M. S. *Prog. Solid State Chem.* **1978**, *12*, 41-99.
(11) Friend, R. H.; Yoffe, A. D. *Adv. Phys.* **1987**, *36*, 1-94.
(12) Beal, A. R.; Liang, W. Y. *Philos. Mag.* **1973**, *27*, 1397-1416. Acrivos, J. V.; Salem, J. R. *Philos. Mag.* **1974**, *30*, 603-619.
(13) Gamble, F. R.; Osiecki, J. H.; Cais, M.; Pisharody, R.; Di Salvo, F.; Geballe, T. H. *Science* **1971**, *174*, 493-497. Subbarao, G. V.; Shafer, M. W.; Tsang, J. C. *J. Phys. Chem.* **1975**, *79*, 553-557.
(14) Riekel, C.; Fischer, C. O. *J. Solid State Chem.* **1979**, *29*, 181-190. Kashihara, Y.; Nishida, A.; Ohshima, K.; Harada, J.; Yoshioka, H. *J. Phys. Soc. Jpn.* **1979**, *46*, 1393-1394.
(15) Tofield, B. C.; Wright, C. J. *Solid State Commun.* **1977**, *22*, 715-718.

0002-7863/92/1514-7792$03.00/0

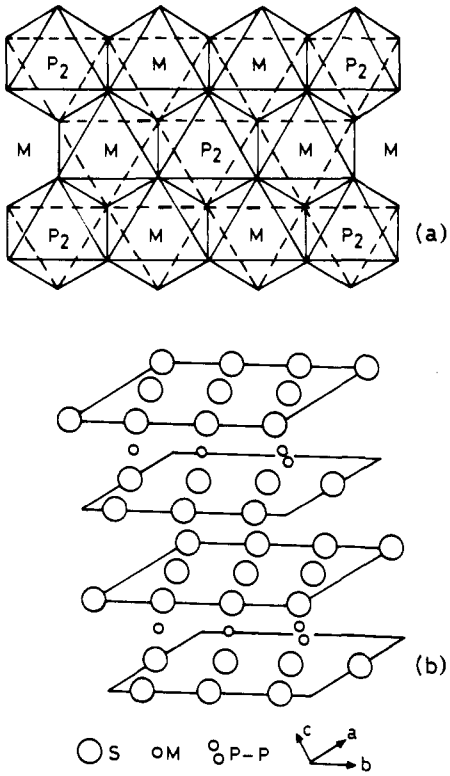

Figure 1. Structure of MPS_3. (a) In-plane structure showing the honeycomb arrangement of metal atoms. The structure is obtained by replacing every third metal atom of a transition metal dichalcogenide layer by a P_2 pair. (b) Stacking of the MPS_3 layers to form the monoclinic space group $C_{2/m}$. The van der Waals gap between the layers is 3.2 Å.

model.[16] The key step in this model is the condensation of two pyridine (pyr) molecules to give 4,4′-bipyridyl with the release of two protons and two electrons. The latter are transferred to the host lattice. The condensation reaction provides the source of protons for the formation of pyridinium ions ($pyrH^+$).

$$x\,\text{pyr} \rightarrow (x/2)\,\text{pyr-pyr} + x\,H^+ + x\,e^-$$

$$x\,\text{pyr} + x\,H^+ \rightarrow x\,\text{pyrH}^+$$

$$MX_2 + x\,\text{pyrH}^+ + y\,\text{pyr} + x\,e^- \rightarrow (MX_2)^{x-}(\text{pyrH}^+)_x(\text{pyr})_y$$

The stability of the intercalated compounds in this model is ascribed to the electrostatic interaction between the negatively charged lattice and pyridinium ions. The pyridinium ions are solvated by neutral pyridine, which helps in screening out the repulsive potentials. There is considerable experimental evidence for many aspects of the above model, especially the existence of solvated pyridinium cations.[16] There has, however, been no direct in situ evidence as yet for the formation of 4,4′-bipyridyl.

An extension of the above model to the MPS_3 compounds would require the transition metals to be reduced still further from their stable +2 state. Alternatively, intercalation may proceed by reduction of a site other than the metal, e.g., either the P–P or P–S linkages, or it may proceed by a totally different mechanism as in the case of the intercalation of organometallics in transition metal thiophosphates.[17] In the latter reaction, the intercalation of a cationic organometallic species into the van der Waals gap is charge compensated by the removal of a corresponding number of metal ions from the host lattice. This situation may be compared with the intercalation of the ionic FeOCl. Here, however, the reduction of part of the Fe^{3+} sites to Fe^{2+} may easily be conceived of.[18]

In the present work we have attempted intercalating pyridine in the transition metal thiophosphates and in particular in $MnPS_3$. The ease of intercalation was found to be $MnPS_3 \gg FePS_3 >>> NiPS_3$. In fact pyridine intercalation was never observed in $NiPS_3$. Since $MnPS_3$ was relatively the easiest to intercalate, with single phase materials being readily obtained, only the intercalated $MnPS_3$ was subjected to a detailed investigation. The manganese compound has the added advantage of the crystals being transparent green ($FePS_3$ and $NiPS_3$ being black in color), making it amenable for spectroscopic studies. In addition, the magnetic susceptibility of $MnPS_3$ is the simplest of the three. The magnetic susceptibility is isotropic and the magnetic interactions may be described by the symmetric isotropic Heisenberg exchange Hamiltonian.[19]

There are brief reports in the literature on the stoichiometry and lattice expansion on pyridine intercalation in $MnPS_3$. Direct intercalation of neutral pyridine was found to lead to a lattice expansion of 5.9 Å,[20] whereas the intercalation of pyridinium cations from aqueous solution was found to proceed via an ion exchange mechanism with a lattice expansion of 3.15 Å.[21] In the case of $MnPSe_3$ it had been reported that a 3.3-Å phase was obtained by the loss of pyridine from the original 5.9-Å phase.[22] The objective of the present work was to try and unravel the nature of host–guest interactions and to understand the accompanying changes in structure and properties of the host lattice.

A comparative investigation of the electrical, optical, vibrational, EPR, and magnetic properties of $MnPS_3$ and pyridine intercalated $MnPS_3$ has been carried out, and the nature of the intercalated species has been probed by vibrational spectroscopy and thermal deintercalation. The intercalated species were, indeed, found to be pyridinium ions solvated by neutral pyridine molecules, but charge balance was not by electron transfer to the host lattice but by a novel ion-exchange/intercalation process in which charge neutrality is maintained by a loss of Mn^{2+} ions. The experimental evidence leading to this conclusion is discussed, and it is shown that the proposed mechanism can consistently explain the observed changes in the electrical, magnetic, and optical behavior arising from the intercalation of pyridine.

II. Experimental Section

The transition metal thiophosphates, MPS_3 (M = Mn, Fe, Ni), were synthesized from the corresponding elements (99.99%), as has been reported earlier.[3] The reaction was carried out in vacuum sealed (10^{-5} Torr) quartz ampules at 873 K, for a period of 2 weeks. Single crystals were grown by the chemical vapor transport method,[23] using a slight excess of sulfur as the transporting agent. The charge end of the vacuum sealed sample tube was maintained at 923 K and the cold end at 873 K. Reasonably sized (5 mm × 5 mm × 0.1 mm) platelet like crystals with well-developed hexagonal morphology were obtained in 2 weeks. The polycrystalline samples and the ground crystals were characterized by powder X-ray diffraction. Powder XRD patterns were recorded on a Philips (Model PW 1050) X-ray diffractometer using Cu Kα radiation (λ = 1.5418 Å). The patterns were indexed in the monoclinic space group $C_{2/m}$. Lattice parameters were computed by a least-squares refinement of the observed reflections. The calculated parameters are a = 6.101 Å (6.077 Å), b = 10.570 Å (10.524 Å), c = 6.828 Å (6.796 Å), and β = 107.31° (107.35°). The numbers in parentheses are the lattice parameters reported in ref 24.

Pyridine as well as substituted pyridines (picolines) were intercalated by sealing, under vacuum, $MnPS_3$ powder or single crystals in contact with freshly distilled pyridine/picolines. For pyridine intercalation, the ampules were maintained at 333 K for a period of 2 weeks, while for the substituted pyridines, complete intercalation was achieved after 4 weeks

(16) Schöllhorn, R.; Zagefka, H. D.; Butz, T.; Lerf, A. *Mater. Res. Bull.* **1979**, *14*, 369–376.
(17) Michalowicz, A.; Clement, R. *Inorg. Chem.* **1982**, *21*, 3872–3877.
(18) Fatseas, G. A.; Palvadeau, P.; Venien, J. P. *J. Solid State Chem.* **1984**, *51*, 17–37. Eckert, H.; Herber, R. H. *J. Chem. Phys.* **1984**, *80*, 4526–4540.
(19) Joy, P. A.; Vasudevan, S. *Phys. Rev. B* **1992**, *46*, in press.
(20) Hangyo, M.; Nakashima, S.; Mitsuishi, A.; Kurosawa, K.; Saito, S. *Solid State Commun.* **1988**, *65*, 419–423.
(21) Clement, R. *J. Chem. Soc., Chem. Commun.* **1980**, 647–648.
(22) Otani, S.; Shimada, M.; Kanamaru, F.; Koizumi, M. *Inorg. Chem.* **1980**, *19*, 1249–1251.
(23) Nitsche, R.; Wild, P. *Mater. Res. Bull.* **1970**, *5*, 419–424. Taylor, B.; Steger, J.; Wold, A. *J. Solid State Chem.* **1973**, *7*, 461–467.
(24) Ouvrard, G.; Brec, R.; Rouxel, J. *Mater. Res. Bull.* **1985**, *20*, 1181–1189.

at 373 K. The powder as well as crystals showed considerable swelling on intercalation. The materials, however, showed no change in color, both intercalated as well as host compounds being green in color. The supernatent pyridine liquid also remained colorless after intercalation. The samples were dried in argon and the extent of intercalation checked by XRD. Absence of the 00*l* reflections of the host, $MnPS_3$, was considered as evidence for complete intercalation. Stoichiometry was established by TGA and by CHN analysis. TG of the intercalated powders as well as crystals showed a single step weight loss at 423 K. The total weight loss was 23%. If the entire loss of weight was due to the deintercalation of pyridine, it would correspond to 0.68 mol of intercalated pyridine for every mol of $MnPS_3$. The molecular formula may, thus, be written as $MnPS_3(pyr)_{2/3}$. (The reported[20] pyridine intercalated compound, $MnPS_3(pyr)_{4/3}$, showed a two-step weight loss in the TG profile. The first weight loss showed a continuous decrease above room temperature and is likely to be due to an incomplete drying of the sample. The Raman spectra of this compound was assigned to physisorbed and chemisorbed pyridines.) CHN analysis gave C 14.76% (17.3%), H 1.30% (1.44%), and N 3.56% (4.0%). The numbers in parentheses are those calculated for $MnPS_3(pyr)_{2/3}$. The origin of this discrepancy is discussed in a later section. The addition of sulfur to the pyridine in the preparation of intercalated samples had no effect on the TG of the intercalated $MnPS_3$—a single step weight loss of 23% being observed and thus confirming that there is no loss of sulfur during intercalation. Thermogravimetric analysis was carried out using a Ulvac Sinku-Rico TA1500 simultaneous TG-DTG-DTA thermal analyser in a flow of dry oxygen free N_2. Elemental analysis (C, H, N) was performed on a Heraeus CHNorapid CHN analyzer.

The manganese content in the supernatant pyridine liquid was determined by spectrophotometry. The supernatant pyridine liquid was dissolved in water and free pyridine was removed from the solution by extraction with chloroform in a separating funnel. Mn^{2+} in the aqueous phase was estimated as the permanganic acid.[25] The solid intercalate was dissolved in nitric acid and the manganese content determined as discussed above.

Electrical conductivities between 77 and 300 K were measured on pressed pellets of the powder samples by an ac two-probe technique using a Wayneker B642 autobalance universal bridge operating at 1591.8 Hz ($\omega = 10^4$ Hz).

Optical absorption spectra of single crystals were recorded in the transmission mode with a Hitachi U3400 recording spectrophotometer. Crystals were fixed on an optically polished quartz disk with Nujol and mounted inside a Specac P/N 21.000 variable-temperature cell. The crystal *ab* plane was perpendicular to the incident beam ($\vec{E} \perp \vec{c}$). Spectra were recorded at 300 and 120 K. A blank run was performed at these temperatures without the crystal to correct for any background effect.

The magnetic susceptibility of crystals in the temperature range 55–375 K was measured using a EG&G PAR vibrating sample magnetometer (VSM), Model 155. Crystals of the sample were attached to the end of a wedge-shaped Teflon piece. The magnetometer was calibrated with $Hg[Co(NCS)_4]$ as standard. In the magnetic susceptibility measurements, $\chi_\parallel$ is defined as the susceptibility with the external magnetic field perpendicular to the *ab* plane (the layer). The definition is similar for both pure and intercalated $MnPS_3$. EPR spectra of single crystals were recorded on an X-band Varian E109 E-line century series EPR spectrometer.

Infrared spectra (3500–100 cm^{-1}) were recorded on a Bruker IFS 113-V FTIR spectrometer. For IR measurements on single crystals, thin crystal platelets were sandwiched between two 0.2-mm-thick high-density polyethylene disks and clamped in the copper block of a Specac P/N 21.000 variable-temperature assembly. The lowest temperature attained was 120 K. Single-crystal spectra were recorded with the electric vector of the incident infrared radiation perpendicular to the *c* axis ($\vec{E} \perp \vec{c}$), so that only IR active normal modes which have a change in dipole moment within the layer would be observed. Raman spectra were recorded by placing the powders in a glass capillary using a Spex 1403 double spectrometer excited by the 488-nm line of an Ar ion laser (Spectra Physics).

Temperature-Programmed Deintercalation Spectra (TPDS). This technique is identical to thermal desorption spectroscopy (TDS). The intercalated samples are heated at a linear rate and the volatile deintercalating molecules analyzed by a mass spectrometer. The temperature at which the rate of appearance of a gaseous species is at a maximum is a measure of the activation barrier for deintercalation or for the formation of the species within the layer. The appearance of more than one peak in the temperature profile is indicative of intercalated species with different strengths of interaction or different rates of reaction/formation. The output of the experiment is a temperature profile for each deintercalating mass (counts vs temperature for each deintercalating m/e). The sum of the counts for each m/e vs temperature; the total number of ion counts (TIC) vs temperature gives information complementary to a TG run. In a TG run, the weight loss is recorded as a function of temperature, whereas in the TPDS, the amount of gaseous products evolving as a function of temperature is monitored. The main advantage of the TPDS is that the gas evolved can be analyzed for different masses, so that the composition of different products as a function of temperature can be monitored.

TPDS studies were done in a modified GC-MSD system, HP 5890-5970. In a TPDS experiment, the intercalated samples were heated at a constant heating rate, 10 K/min (300–675 K), in a stream of helium. The volatile deintercalating products in the mass range m/e = 10 to 400 were analyzed online using a quadrupole mass spectrometer. The data were collected on a HP9000, 200 series computer. In a typical TPDS run, the intercalated material was placed in a thin-walled stainless steel tube. The tube occupied the same position as the column in the GC and was connected to the MS by a silicone capillary. The other end of the tube was connected to a He cylinder using the gas plumbing provided in the GC. The temperature of the oven was controlled to ±1 K by the control circuit provided in the GC, which also provided variable linear rates of heating.

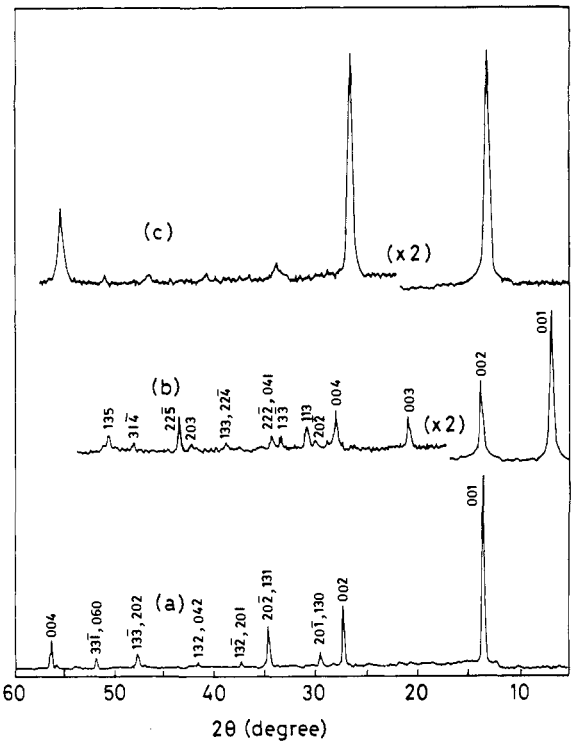

Figure 2. X-ray powder diffraction patterns of (a) $MnPS_3$, (b) $MnPS_3(pyr)_{2/3}$, and (c) $MnPS_3$ obtained from thermal deintercalation of $MnPS_3(pyr)_{2/3}$.

Table I. Calculated Unit Cell Parameters of $MnPS_3$ and $MnPS_3(pyr)_{2/3}$

lattice parameter	$MnPS_3$	$MnPS_3(pyr)_{2/3}$
a (Å)	6.101	6.064
b (Å)	10.570	10.548
c (Å)	6.828	13.063
β (deg)	107.31	107.00

III. Results and Discussion

Structure. The powder XRD of $MnPS_3(pyr)_{2/3}$ is shown in Figure 2. For comparison, the XRD of the unintercalated host is also shown. It may be seen that the 00*l* reflections of $MnPS_3$ are totally absent in the intercalated samples. New 00*l* reflections are observed with a lattice spacing of 12.4 Å, corresponding to a lattice expansion (Δd) of 5.9 Å. The XRD of $MnPS_3(pyr)_{2/3}$ could be indexed in the $C_{2/m}$ space group, assuming that the only change from the parent $MnPS_3$ structure is an expansion of the *c* axis. The calculated *a*, *b*, and β values are almost identical with that of pure $MnPS_3$ and are given in Table I. It was not, however,

(25) Vogel, A. I. *A Textbook of Quantitative Inorganic Analysis*; Longman: London, 1969.

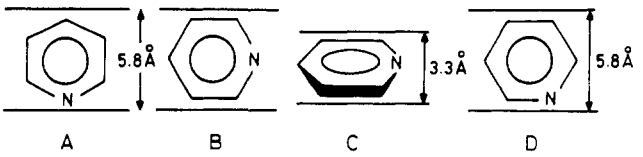

Figure 3. Four possible orientations of pyridine molecules between the $MnPS_3$ layers. Expected lattice expansion is given for each orientation.

Table II. Observed *d*-Spacings and Stoichiometry of Pyridine and Substituted Pyridines Intercalated in $MnPS_3$

compound	*d* (Å)	Δ*d* (Å)	*x*
$MnPS_3$	6.5		
$MnPS_3$(pyridine)$_x$	12.4	5.9	0.67
$MnPS_3$(γ-picoline)$_x$	12.3	5.8	0.58
$MnPS_3$(β-picoline)$_x$	13.5	7.0	0.55
	12.35	5.85	

possible to refine the intensities to get further structural information, because of the strong preferred orientation of the crystallites. Attempts to solve the structure of single crystals of $MnPS_3(pyr)_{2/3}$ were also not successful since the crystals showed considerable mosaic. Thus, the Weisenberg photographs showed spots only for the 00*l* reflections, while the other reflections appeared as streaks.

The XRD pattern of $MnPS_3$(γ-picoline)$_x$ showed a lattice expansion of 5.80 Å, comparable to that for $MnPS_3(pyr)_{2/3}$. Samples of $MnPS_3$(β-picoline)$_x$ were found to be biphasic, with two sets of 00*l* reflections being observed. The phases correspond to compounds with lattice expansion (Δ*d*) of 7.0 and 5.9 Å, respectively. The *a*, *b*, and β parameters for the substituted pyridine samples were comparable to that of the pyridine intercalated as well as to that of pure $MnPS_3$. The observed lattice expansion and the stoichiometry of the pyridine and substituted pyridine samples are given in Table II.

The XRD of the thermally deintercalated samples (heating in vacuum at 523 K) showed complete recovery of the original host structure. Figure 2 shows the XRD patterns for $MnPS_3$, $MnPS_3(pyr)_{2/3}$, and the thermally deintercalated sample. Apart from line broadening, the XRD of the deintercalated sample is identical with that of pure $MnPS_3$. The line broadening occurred due to the breaking up of the crystallites during the intercalation–deintercalation process. The intercalation thus appears to be topotactic and reversible.

It was observed that when the intercalated samples were exposed to the atmosphere they underwent a slow transformation to a phase characterized by a new set of 00*l* reflections in the XRD. The new *d*-spacing was 9.9 Å, corresponding to a lattice expansion of 3.4 Å, with all other lattice parameters remaining the same. This new phase has the same green color as the freshly prepared compound, $MnPS_3(pyr)_{2/3}$. The thermal deintercalation of the new phase gave back the original $MnPS_3$ phase. This transformation was much more facile for powders as compared to the intercalated crystals. The TG, however, now showed a two-step weight loss at 365 and 425 K with an overall weight loss of 21%. The fact that the TG shows a weight loss at 365 K suggests the incorporation/exchange of H_2O molecules from the atmosphere.

The electrical and magnetic properties as well as the optical and EPR spectra of the phase characterized by a lattice expansion of 3.4 Å (henceforth called the 3.4-Å phase) showed no difference from the original intercalated compound (henceforth called the 5.9-Å phase) and are not described separately. Measurements on the 3.4-Å phase were done on powder samples so that the spectral resolution was much poorer. Only in situations where differences were observed are details given.

Orientation. A pyridine molecule within the van der Waals gap in $MnPS_3$ could, in principle, have any of the four orientations[26] shown in Figure 3. The observed lattice expansion (5.9 Å) rules out **C** as a possible orientation. The fact that the intercalation of 4- and 3-methyl-substituted pyridines gave lattice expansions of 5.8 and 7.0 Å, respectively, implies that the orientation of the pyridine molecule is **B**. Only this orientation leaves the lattice expansion unaffected for substitution at the 4-position. It is interesting to note that this orientation is similar to that reported in the transition metal dichalcogenides.[27] Substitution at either the 2- or 3-positions would cause an additional expansion proportional to the size of the substituent. The additional 5.9-Å phase observed for the 3-methylpyridine intercalated sample may correspond to orientation **D**. The lattice expansion of the air-exposed samples (3.4-Å phase) suggests that orientation of the pyridine molecules may have changed to **C** from **B**, the observed lattice expansion being close to the thickness of the pyridine molecule.

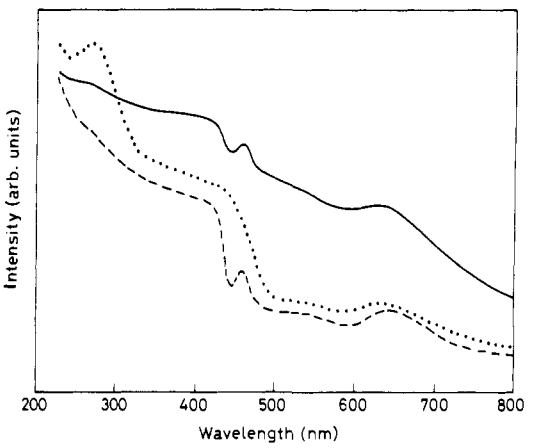

Figure 4. Optical absorption spectra of single crystals: (—) $MnPS_3(pyr)_{2/3}$ at 120 K, (···) $MnPS_3$ at 300 K, (---) $MnPS_3$ at 120 K.

Table III. Calculated (with B = 560 cm^{-1}, C = 3250 cm^{-1}, Dq = 850 cm^{-1}) and Observed Transition Energies for $MnPS_3$ and $MnPS_3(pyr)_{2/3}$ with Assignments

calcd transition energy (cm^{-1})	obsd transition energy (cm^{-1})		assignments
	$MnPS_3$	$MnPS_3(pyr)_{2/3}$	
15780	15723	15750	$^6A_{1g} \rightarrow {}^4T_{1g}(G)$
18830	19417	19330	$^6A_{1g} \rightarrow {}^4T_{2g}(G)$
21850	21834	21910	$^6A_{1g} \rightarrow {}^4A_{1g}$ & $^4E_g(G)$
	22700	22758	charge transfer
24100			$^6A_{1g} \rightarrow {}^4T_{2g}(D)$
25770			$^6A_{1g} \rightarrow {}^4E_g(D)$
31337			$^6A_{1g} \rightarrow {}^4T_{1g}(P)$
35070			$^6A_{1g} \rightarrow {}^4A_{2g}(F)$
36674			$^6A_{1g} \rightarrow {}^4T_{1g}(F)$
	37300	37280	charge transfer
39761			$^6A_{1g} \rightarrow {}^4T_{2g}(F)$

Electrical Properties. The electrical conductivity of $MnPS_3$ is unaffected by intercalation of pyridine. The room temperature resistivities of pure $MnPS_3$ and the intercalated compound are of the order of 10^8 ohm·cm and both compounds showed almost similar temperature dependence. This observation is in contrast to that observed in the transition metal dichalcogenides,[28] where pyridine intercalation is accompanied by fairly large changes in the electrical conductivity—both magnitude and temperature variation. The fact that pyridine intercalated $MnPS_3$ is as electrically insulating as pure $MnPS_3$ implies that if any charge transfer has taken place from the intercalated pyridine it is to localized acceptor states of the host lattice.

Optical Spectra. The optical absorption spectra of the pyridine intercalated $MnPS_3$ show practically no difference from pure $MnPS_3$. The optical absorption spectra ($\vec{E} \perp \vec{c}$) of single crystals of $MnPS_3$ (300 and 120 K) and pyridine intercalated $MnPS_3$ (120 K) are shown in Figure 4. The positions of the bands in the pure compound and the intercalated compound are identical (Table

(26) Whittingham, M. S. *Mater. Res. Bull.* **1978**, *13*, 775–782.

(27) Subbarao, G. V.; Shafer, M. W. In ref 1, pp 99–199.

(28) Klipstin, P. C.; Friend, R. H.; Yoffe, A. D. *Philos. Mag.* **1985**, *B52*, 611–642.

III) and so, too, are the changes associated with temperature. Consequently, the assignment of features in the two compounds would, obviously, be similar. For $MnPS_3$, the temperature-independent features at 635 nm (15748 cm^{-1}), 515 nm (19417 cm^{-1}), and 460 nm (21835 cm^{-1}) have been assigned[29] to the spin-forbidden sextet-quartet $^6A_{1g} \rightarrow {}^4T_{1g}$, $^6A_{1g} \rightarrow {}^4T_{2g}$, and $^6A_{1g} \rightarrow {}^4A_{1g}$, ^4E_g transitions respectively while the temperature-dependent absorption edge at 440 nm (22700 cm^{-1}) and the peak at 268 nm (37300 cm^{-1}) originate from ligand-to-metal charge transfer. The crystal field bands have been interpreted in the weak field limit of crystal field theory.[30] The Racah interelectron repulsion parameters B and C as well as the crystal field splitting parameter, Dq, were evaluated from the appropriate weak field matrices.[31] For both $MnPS_3$ and the intercalated compound, the parameters are Dq = 850 cm^{-1}, B = 560 cm^{-1}, and C = 3250 cm^{-1}. In an earlier publication,[29] we have interpreted the large value of the Racah B parameter as being due to a fairly ionic environment for Mn in $MnPS_3$. The fact that the Racah B as well as the Dq parameters are unchanged on intercalation implies that the crystal field and the ionic nature of the M–S bond are identical with those in the pure compound.

The optical spectra of the intercalated samples show that very little or practically no change has occurred in the d electron levels of the manganese ion, even after intercalation. What is surprising is that there is no change—even in the position of the ligand-to-metal charge-transfer band (the sharp edge at 440 nm). The charge-transfer band would be expected to be sensitive to the filling of the d band, e.g., the transition metal dichalcogenides show a pronounced blue shift on intercalation.[32]

EPR Studies. Since the optical spectra would not be sensitive to small concentrations (<10%) of manganese in a different oxidation state, a more concentration sensitive technique, like EPR, was employed. Here, too, however, no changes were observed. The position of the resonance of the pyridine intercalated $MnPS_3$ and that of pure $MnPS_3$ crystals is identical (g = 2.004) and no additional features are observed. The line width is different for the $MnPS_3(pyr)_{2/3}$ crystals as compared to $MnPS_3$.[33] The EPR results confirm that there is no change in the oxidation state of the Mn^{2+} nor any change in the crystal field felt by the ion, even after intercalation.

Magnetic Susceptibility. The temperature variation of the magnetic susceptibility of single crystals of $MnPS_3$ and pyridine intercalated $MnPS_3$ is shown in Figure 5. Single crystal measurements were done with the applied field parallel ($\chi_\perp$) and perpendicular ($\chi_\parallel$) to the layers. As may be seen from the figure, intercalation causes a drastic difference in the susceptibility behavior. The low-temperature transition to an antiferromagnetic state (Neel temperature, T_N = 78 K) in pure $MnPS_3$ is now no longer observed and instead the intercalated material shows weak ferromagnetism below 70 K. The ferromagnetic transition temperature, T_c, is 60 K. The magnetic behavior of the powder samples of the 3.4-Å phase was identical. A similar magnetic behavior is reported for the cobaltocene intercalated compounds of $MnPS_3$.[34] For the pure host the susceptibility in the paramagnetic region (above 120 K) is isotropic while for the intercalated compound it is isotropic over the entire temperature range.

The magnetic susceptibility of $MnPS_3$ is typical of antiferromagnetic ordering. Figure 5a shows that for $MnPS_3$ the antiferromagnetic axis is collinear with the trigonal axis in agreement with the neutron diffraction studies.[35] Above 200 K the susceptibility of $MnPS_3$ obeys a Curie–Weiss law with a Weiss constant (Θ) of −160 K and an effective magnetic moment (μ_{eff})

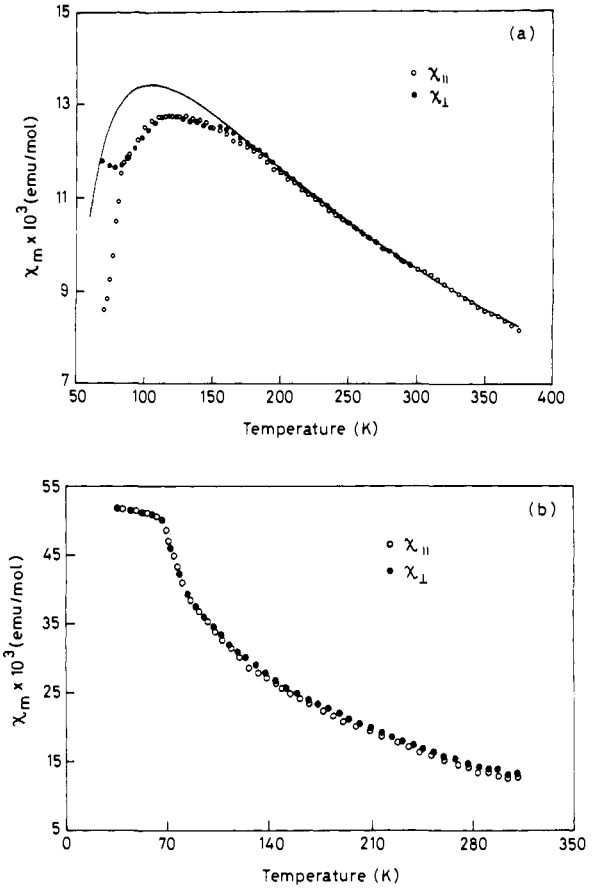

Figure 5. (a) Magnetic susceptibility of $MnPS_3$ single crystals parallel ($\chi_\parallel$) and perpendicular ($\chi_\perp$) to the trigonal axis as a function of temperature. The solid line is the calculated susceptibility using the high-temperature series expansion expression, $\chi = Ng^2\beta^2S(S+1)[1 + \Sigma_1^6(-1)^n b_n(J/T)^n]^{-1}/3kT$ with J = −8.1 K and g = 2.010. b_n's are the expansion coefficients for a two-dimensional honeycomb lattice as derived from ref 36. (b) Magnetic susceptibility of pyridine-intercalated $MnPS_3$ crystal both parallel ($\chi_\parallel$) and perpendicular ($\chi_\perp$) to the trigonal axis as a function of temperature.

of 5.97 μ_B which is close to the spin only value of 5.90 μ_B, expected for a high-spin d^5 ion. The isotropy of the paramagnetic susceptibility of $MnPS_3$ suggests that it is best described by the isotropic Heisenberg exchange Hamiltonian. Consequently the exchange constant, J, was evaluated[19] by fitting the experimental data to the theoretical high-temperature series expansion expression of the susceptibility of a two-dimensional isotropic Heisenberg antiferromagnet, as given by Rushbrooke and Wood.[36] The best fit was obtained for J/k = −8.1 K and g = 2.010.

For the pyridine intercalated crystals the susceptibility in the paramagnetic region could be fitted to a Curie–Weiss law with μ_{eff} = 6.3 μ_B and Θ = −90 K. No anisotropy is observed for single crystals over the entire temperature range. The fact that the Weiss constant is strongly negative implies antiferromagnetic interaction between the manganese ions, and consequently the weak ferromagnetism must arise either from a canted antiferromagnetic structure or ferrimagnetism. The latter may be ruled out since the EPR does not show evidence for manganese ions in any other oxidation state, apart from +2. In the canted antiferromagnetic structure, the canting of spins causes an incomplete cancellation of magnetization of the various antiferromagnetic sublattices, so that there is a residual ferromagnetism.[37] Two mechanisms are known which can give rise to a canting of spins. (i) The first mechanism is the Dzyaloshinsky–Moriya (DM) antisymmetric exchange, $d_{ij} \cdot S_i \times S_j$, which causes the spins i and j to align per-

(29) Joy, P. A.; Vasudevan, S. *Phys. Rev. B* **1992**, *46*, in press.
(30) Griffith, J. S. *The Theory of Transition Metal Ions*; Cambridge University Press: Cambridge, 1961.
(31) Orgel, L. E. *J. Chem. Phys.* **1955**, *23*, 1004–1014.
(32) Gamble, F. R.; Di Salvo, F. J.; Klemm, R. A.; Geballe, T. H. *Science* **1970**, *168*, 568–570.
(33) Joy, P. A.; Vasudevan, S. To be submitted for publication.
(34) Clement, R.; Girerd, J. J.; Morgenstern-Badarau, I. *Inorg. Chem.* **1980**, *19*, 2852–2854.
(35) Kurosawa, K.; Saito, S.; Yamaguchi, Y. *J. Phys. Soc. Jpn.* **1983**, *52*, 3919–3926.
(36) Rushbrooke, G. S.; Wood, P. J. *Mol. Phys.* **1958**, *1*, 257–283.
(37) Moriya, T. In *Magnetism*; Rado, G. T., Suhl, H., Eds.; Academic: New York, 1963; Vol. I, pp 85–125.

pendicular to each other. This mechanism is operative only if spins i and j are not related by a center of inversion. (ii) The second mechanism involves different single ion anisotropies $D_1S_{1z}^2$ and $D_2S_{2z}^2$ in the two sublattices of the antiferromagnetic systems. A canted structure may be realized if $D_1 \neq D_2$ and the easy axes of the two sites are in different directions.

It is difficult to understand how mechanism ii could be operative since none of the measurements—optical, magnetic, and EPR—gave any evidence for Mn^{2+} ions with different single ion anisotropies. The magnetic susceptibility of the intercalated compound showed no anisotropy nor did the EPR show any additional feature as compared to pure $MnPS_3$. Moreover, the XRD of the intercalated samples seems to suggest that the center of inversion of $MnPS_3$ is preserved even after intercalation. XRD of the intercalated sample could be indexed in the $C_{2/m}$ space group with the only change from $MnPS_3$ being in the c-axis lattice parameter. Consequently it is puzzling how a canted structure can be realized even by the DM exchange mechanism.

Another puzzling feature is the isotropy of the low-temperature, weakly-ferromagnetic state. In other systems where a canted state is known, e.g., NiF_2 or Fe_2O_3,[37] weak ferromagnetism is observed only in a perpendicular direction, whereas in the other direction it behaves as a normal antiferromagnet. For example, in NiF_2, $\chi_\perp$ shows a sharp increase near T_N while $\chi_\parallel$ decrease with decreasing temperature as in a normal antiferromagnet. If in the intercalated $MnPS_3$ lattice the spins were canted away from the trigonal axis (the antiferromagnetic axis of pure $MnPS_3$), then one would have observed an increase in susceptibility for $\chi_\perp$ near T_N whereas for $\chi_\parallel$ it should have decreased below T_N, since the components of the spins along the trigonal axis for each sublattice would cancel each other. Only in situations where the canting angle is different for different sublattices (so that in no direction is the cancellation of moments complete) would the present observation—increase in susceptibility for both $\chi_\parallel$ and $\chi_\perp$ near T_c—be realized.

Vibrational Spectra. None of the measurements discussed so far have given any indication of the type of interaction between the pyridine molecules and the host lattice, nor any evidence for charge transfer of electrons from pyridine to $MnPS_3$, since no other oxidation state of manganese apart from Mn^{2+} is observed. However, there could be other reduction sites in the $MnPS_3$ structure such as the P–P or the P–S bonds which could, perhaps, accept an additional electron. Reduction of such centers would lead to fairly drastic and easily observable changes in the vibrational spectra. It had been shown[38] from the orientation dependence and by a comparative study of the vibrational spectra of the transition metal thiophosphates that their lattice vibrations in the 100–700-cm^{-1} region is separable into that of the normal modes of the "ethane-like" P_2S_6 group and the external modes which are due to the M–S vibrations. The latter appears in the 250–280-cm^{-1} region (256 cm^{-1} in $MnPS_3$) and has been assigned to the F_{1u} vibration of the MS_6 octahedra. The bands in the 600–300-cm^{-1} region have been assigned to the IR active normal modes of the "ethane-like" P_2S_6 group. The finer details in the vibrational spectra were shown to originate from correlation and factor group splittings. $MnPS_3$ possesses a center of inversion and the IR and Raman modes are mutually exclusive. The fact that the normal modes are separable implies that any reduction of the P–P or P–S linkages would be easily observable and identifiable.

The vibrational spectrum of $MnPS_3(pyr)_{2/3}$ is discussed in two parts—the first dealing with the lattice vibrations occurring in the 100–700-cm^{-1} region, where the vibrational modes of $MnPS_3$ were observed, and the second due to the normal modes of vibration of the intercalated pyridine (700–3500 cm^{-1}). It was found that the spectrum in the 700–3500-cm^{-1} region of the 3.4-Å phase was quite different from that of the 5.9-Å phase whereas in the 100–700-cm^{-1} region they were identical.

(i) Lattice Vibrations (700–100 cm^{-1}). The infrared spectra of $MnPS_3(pyr)_{2/3}$ crystals along with the pure $MnPS_3$ spectra are shown in Figure 6, and the positions of the various features are given in Table IV. An examination shows that most of the intense features of the $MnPS_3$ spectrum continue to be present even after intercalation. The Raman spectrum of the intercalated compound is also shown in Figure 6. The spectrum is identical with that of the pure compound. The Raman spectra were in general of poor quality with a low signal-to-noise ratio. Consequently the discussion is restricted only to the IR vibrational spectra. Only the most intense Raman bands are shown in the figure. The assignments of the IR vibrational spectra are identical with that for the pure MPS_3 compounds and are indicated in Table IV. The spectra show that vibrational features in the 600–400-cm^{-1} region, which were assigned to the P–S stretching frequencies[38] of the P_2S_6 unit of the $M_2P_2S_6$ lattice, remain unaffected on intercalation. The correlation and factor group splittings appear to be of the same order as in the pure MPS_3 compounds. The Mn–S stretching vibration at 256 cm^{-1} too remains unchanged in agreement with the optical and EPR measurements, which show no change in the oxidation state of the manganese ion.

The IR spectrum of the intercalated sample shows a number of additional features as compared to that for the $MnPS_3$ crystal (Figure 6). The features at 512 and 348 cm^{-1}, however, have been observed in the IR spectrum of $MnPS_3$ powder as well as in the powder and crystal spectra of $FePS_3$ and $NiPS_3$.[38] Intercalation appears to have enhanced the oscillator strengths of these features. The sharp band at 385 cm^{-1} is a new feature. It may, however, be seen that at 385 cm^{-1} it is the most intense feature in the Raman spectra of $MnPS_3(pyr)_{2/3}$. It may also be observed that the intense Raman band at 280 cm^{-1} appears as a shoulder in the $MnPS_3(pyr)_{2/3}$ single-crystal IR vibrational spectrum. The presence of Raman active bands in the IR spectrum implies that the intercalated structures no longer possess a center of inversion. This may be due to a distortion of either the MS_6 or P_2S_6 octahedra on intercalation. Since the positions of the IR bands of

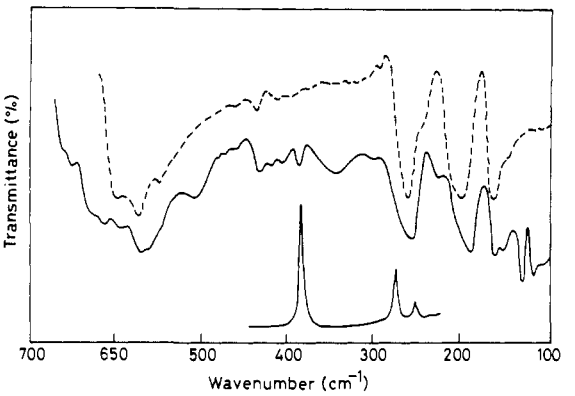

Figure 6. Infrared spectra (lattice vibrations) of crystals of $MnPS_3(pyr)_{2/3}$ (—) and pure $MnPS_3$ (---) at 120 K. The first three intense Raman bands of the intercalated sample are shown at the bottom.

Table IV. Infrared Vibrational Frequencies (in cm^{-1}) of Crystals of $MnPS_3$ and $MnPS_3(pyr)_{2/3}$ at 120 K[a]

$MnPS_3$	$MnPS_3(pyr)_{2/3}$	assign	$MnPS_3$	$MnPS_3(pyr)_{2/3}$	assign
593 m	595 m	ν_7 (A_u)	302 m	304 br	
571 s	573 w	ν_7 (A_u)	285 sh	280 sh	
564 w	564 w	ν_7 (B_u)	256 vs	258 vs	F_{1u}
545 s	546 sh	ν_7 (B_u)		227 w	
	512 br		206 sh	210 sh	
	484 w		192 s	191 s	
	477 w		166 s	163 s	
464 w	463 w		155 sh	154 w	
453 w	456 vw	ν_6 (B_u)		131 s	
428 s	430 s	ν_7 (A_u + B_u)	118 w	117 s	
	423 w		107 w	109 w	
413 w	411 w				
	385 s				
	348 br				

[a] w, weak; m, medium; br, broad; sh, shoulder; s, strong; vs, very strong.

(38) Joy, P. A.; Vasudevan, S. *Phys. Rev. B.* Submitted for publication.

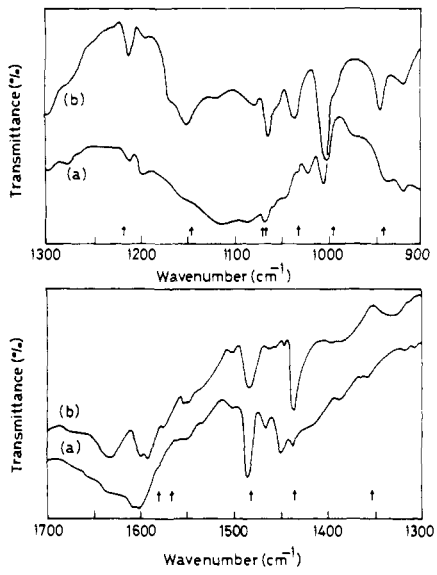

Figure 7. Infrared spectra (pyridine modes) of pyridine intercalated $MnPS_3$ crystals: (a) 5.9-Å phase and (b) 3.4-Å phase. The arrows indicate the position of liquid pyridine bands.

$MnPS_3(pyr)_{2/3}$ are identical with those of $MnPS_3$, these distortions must indeed be very small (in the parent $C_{2/m}$ space group, all degeneracies are already lifted so that lowering of symmetry to a space group which does not possess a center of inversion would not lead to any additional splittings).

The vibrational spectra show that, apart from the loss of center of symmetry, most other features (positions, intensities, etc.) remain unchanged, suggesting that there is very little change in the nature of bonding between the metal and the P_2S_6 ligand after intercalation and not much change in the bonding within the P_2S_6 group. The fact that the intercalated compound no longer possesses a center of symmetry means that the structure can support a canted antiferromagnetic state due to DM exchange, giving rise to weak ferromagnetism, which has indeed been observed. One possible reason why the XRD could still be indexed in the $C_{2/m}$ space group is that the magnitudes of the distortions are too small to be observed by such a gross technique as powder XRD.

(ii) Vibrational Modes of Pyridine. The IR spectra of pyridine intercalated $MnPS_3$ have been recorded in the region 700–3500 cm^{-1}, where pyridine modes are known to be active.[39] As mentioned earlier, the spectra of the 5.9-Å phase are quite different from that of the 3.4-Å phase. The spectra of the former were recorded on crystals, whereas for the later the spectra were recorded on powder samples. The spectra of both phases are shown in Figure 7, and the positions of the various absorption frequencies are given in Table V. In Figure 7 the arrows show the position of liquid pyridine bands. The spectra of the two phases show differences, both in the positions and relative intensities of the various bands, suggesting that intercalated pyridine in the two phases has different environments and interactions. Attention has been focused in the regions where the ring stretching modes of the free pyridine occur. In has been well established[40] that the pyridine ring stretching modes at 991 and 1581 cm^{-1}, which are symmetric with respect to the molecular C_2 axis, are extremely sensitive to the nature of interaction of the pyridine molecule—donor–acceptor, hydrogen bonding, etc. A close examination of this region in the spectrum of the 5.9-Å phase shows a strong band at 1005 cm^{-1} with a shoulder at 991 cm^{-1} and a medium intensity band at 1024 cm^{-1}. The bands in the 1581-cm^{-1} region show a similar pattern. The free pyridine band at 1581 cm^{-1} is seen as a shoulder, while the main feature is a doublet (1602, 1609 cm^{-1}) and a weak band at 1635 cm^{-1}. For the 3.4-Å phase of the pyridine-intercalated $MnPS_3$, the pyridine band at 991 cm^{-1} is totally absent. Instead, there is an intense band at 1002 cm^{-1}, and in the 1581-cm^{-1} region the main feature is a doublet at 1593 and 1598 cm^{-1} and a broad band at 1635 cm^{-1}. An additional feature of the IR spectrum of this phase is bands at 3240 and 3263 cm^{-1}, indicative of loosely bound water.

A comparison of the position of the various bands with the literature values[39,40] is shown in Table V. It may be seen that for the 5.9-Å phase the features in the ring stretching region may be accounted for by a combination of pyridinium ion and free pyridine modes. For the 3.4-Å phase, the position of the band at 1002 cm^{-1} indicates much weaker interaction, and in fact the positions of various absorptions compare favorably with those of aqueous pyridine and this is corroborated by the presence of bands due to H_2O at 3240 and 3263 cm^{-1}. It thus appears that the intercalated species are pyridinium ions, solvated by free pyridine molecules. The 3.4-Å phase is probably obtained by the exchange of neutral pyridine molecules in the solvation shell with water molecules from the atmosphere. The origin of pyridinium ions is, however, puzzling, and the present IR spectra do not give any clear indication of either the presence or absence of bipyridyl as suggested by the Schöllhorn model.[16] Even if present, the con-

Table V. Comparison of the Positions of Various Bands (cm^{-1}) of the Infrared Spectra of Pyridine-Intercalated $MnPS_3$ (Vibrational Modes of Pyridine) with Other Known Compounds

	$MnPS_3$–pyridine				
assign[b]	crystal	powder	liquid pyridine	aqueous pyridine[a]	protonated pyridine[b]
C–C, C–N	1635	1635			1631
ring	1609				
stretching	1602				1603
		1598	1598		
		1593		1592	
	1580	1578	1581		
	1555	1555			
	1550				
	1535	1536	1531		1530
	1503	1503			1501
	1485	1485	1483	1486	1481
	1467	1463			
	1450	1447		1444	
	1438	1436	1437		
in-plane	1417				
ring		1398			
deformation	1388	1385			
					1375
	1367				
	1357		1355		
in-plane	1213	1212	1217	1217	
C–H	1199	1198			1198
deformation	1168				1168
	1155	1154	1152	1150	
	1118	1115			
	1085	1080	1072		
	1066	1064		1062	1066
in-plane	1058	1053			1059
ring	1030	1035	1034	1035	
bend	1024				1027
	1005	1002		1002	1005
	991		991		
out-of-plane		975	980		
C–H	943		942		943
deformation	918	919			
out-of-plane					759
ring	749	747	748		
deformation					
out-of-plane	707	702	705		
C–H	686	685			684
deformation					

[a] Sidorov, A. N. *Opt. Spectrosc.* **1960**, *8*, 24–28. [b] Greenwood, N. N.; Wade, K. *J. Chem. Soc.* **1960**, 1130–1141.

(39) Wilmshurst, J. K.; Bernstein, H. J. *Can. J. Chem.* **1957**, *35*, 1183–1194. Filimonov, V. N.; Bystrov, D. S. *Opt. Spectrosc.* **1962**, *12*, 31–35. Sidorov, A. N. *Opt. Spectrosc.* **1960**, *8*, 24–28.

(40) Greenwood, N. N.; Wade, K. *J. Chem. Soc.* **1960**, 1130–1141.

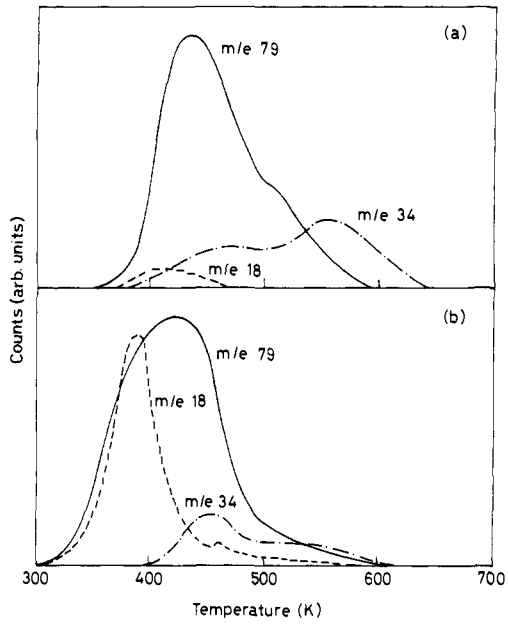

Figure 8. Temperature-programmed deintercalation spectra (TPDS) profiles for pyridine, m/e 79 (—), H_2O, m/e 18 (---), and H_2S, m/e 34 (-·-).

centration of bipyridyl would be very small. The most probable source of protons is trace amounts of water present in the pyridine even after distillation and drying.

Temperature-Programmed Deintercalation Spectra. This technique is identical with thermal desorption spectroscopy. The intercalated samples are heated at a linear rate and the volatile intercalating molecules are analyzed by a mass spectrometer. The output of the experiment is a temperature profile for each deintercalating mass. The appearance of more than one peak in the temperature profile is indicative of intercalated species with different strengths of interaction or different rates of reaction/formation. The thermal deintercalation spectra were recorded for both the 5.9-Å and 3.4-Å phases.

The temperature profiles for a few selected masses—pyridine (m/e = 79), water (m/e = 18), and H_2S (m/e = 34)—are shown in Figure 8 for both phases. For both samples, as expected, the major deintercalating species is pyridine; however, the loss of pyridine is not a single-step process. In fact the pyridine temperature profiles for the two samples are quite different, indicating that the nature of the interactions of the intercalated pyridine molecule is different in the two phases. For the 5.9-Å phase, the pyridine deintercalation profile shows a maximum at 415 K with a pronounced shoulder at ~510 K. There is a small H_2O peak centered around 400 K for this phase. In the 3.4-Å phase, the feature at ~510 K is less well defined and there is an additional feature at low temperature (390 K). It may also be seen that in the 3.4-Å phase a large amount of H_2O is also liberated. The maximum in the H_2O deintercalation profile is at 390 K, which is also the position of the low-temperature pyridine peak of this phase. There is a small H_2O peak at 460 K for the 3.4-Å phase. The most puzzling feature of the deintercalation spectra is that, apart from the expected species pyridine, a fairly large amount of H_2S was detected. The H_2S temperature profile shows two steps (at ~465 and ~550 K for the 5.9-Å phase and at 460 and 500 K for the 3.4-Å phase), but the relative intensities of the two peaks are different for the two phases. In addition to H_2S, small amounts of sulfur (S, m/e = 32; S_2, m/e = 64; S_3, m/e = 96, etc.) and phosphorus sulfides (P_2S, m/e = 95; P_2S_3, m/e = 158, etc.) were also observed. Their intercalation profiles were not complete until 673 K and are not shown in the figure. No mass corresponding to bipyridyl (m/e = 156) was detected.

Many of the features of the thermal deintercalation spectra may be understood (and are in agreement) in light of the vibrational spectra of the intercalated species. For the 3.4-Å phase, the large amount of H_2O liberated at 390 K shows strong association of H_2O molecules with pyridine. The low-temperature feature in the pyridine temperature profile of the 3.4-Å phase at 390 K is probably due to this species. The absence of these features in the deintercalation spectra of the 5.9-Å phase is also in agreement with the IR data. The main peak at 415 K in the pyridine–temperature profile for both phases is due to the deintercalation of the neutral pyridine molecules. It may be recalled that the IR spectra showed the presence of pyridinium ions. Obviously such a charged species cannot deintercalate. Instead the following reaction takes place.

$$2\,pyrH^+ + S^{2-}\ (lattice) \rightarrow 2\,pyr + H_2S$$

This reaction accounts for the peak in the pyridine profile at 510 K and the H_2S temperature profile at ~550 K. When H_2O molecules are also present, an alternate scheme is possible as given below.

$$pyrH^+ + H_2O \rightarrow pyr + H_3O^+$$

$$2\,H_3O^+ + S^{2-}\ (lattice) \rightarrow H_2S + 2\,H_2O$$

The above scheme requires the liberation of H_2S to be associated with the liberation of H_2O. This is probably the major reaction in the 3.4-Å phase. It may be seen that the H_2O–temperature profile shows a well-defined peak at 460 K, identical with that of the first step of the H_2S profile. This is in agreement with the above scheme. For the 5.9-Å phase, the H_2S peak at 465 K is associated with the H_2O evolution seen at 400 K. The origin of this small amount of water in the intercalated compound may be from the exchange of neutral pyridine molecules in the solvation shell with H_2O molecules from the atmosphere. The relative intensities of the two steps in the H_2S profile reflect the relative importance of the two reaction schemes. The results of the thermal deintercalation spectra are in complete agreement with the IR data. For the 5.9-Å phase, pyridine molecules exist as neutral and protonated species, whereas for the 3.4-Å phase, the pyridine molecules are associated with water.

The formation of H_2S by reaction of the intercalated cationic species with the lattice sulfur, as well as the presence of sulfur and phosphorus sulfides in the deintercalation products, implies a partial breaking up of the $MnPS_3$ lattice on deintercalation. It may be recalled that during the intercalation of pyridine no sulfur comes out of the lattice (see Experimental Section). This is confirmed by mass spectral study of the supernatent pyridine where no masses due to sulfur were detected. The presence of sulfur in the thermal deintercalation products is a direct consequence of the deintercalation reaction.

The above observations give rise to a paradoxical situation. The XRD results suggest that the intercalation is truly reversible, since the original $MnPS_3$ diffraction pattern is recovered on thermal deintercalation (Figure 2). The thermal deintercalation product profiles, however, show that the deintercalation reaction is accompanied by a break up of the lattice since sulfur, phosphorus sulfides, and hydrogen sulfide are obtained. The resolution of this paradox is probably the key to the mechanism of the intercalation reaction.

Intercalation of Pyridine in $MnPS_3$: The Mechanism. Any mechanism of the intercalation reaction would have to answer the following two questions. (i) How is charge neutrality maintained? The vibration and the thermal deintercalation spectra confirm that the intercalated species is the solvated cation, $pyrH^+$, but no corresponding reduced site of the host lattice has been observed by electrical and magnetic measurements or by optical, EPR, and lattice vibrational spectra. Moreover, if pyridinium cations are formed by the reaction

$$pyr + H_2O \rightarrow pyrH^+ + OH^-$$

(rather than bipyridyl formation, for which there is no evidence), the mechanism would also have to account for the subsequent fate of the OH^- ions. (ii) Why are the XRD and thermal deintercalation product profile results in contradiction?

A possible mechanism which can account for the above points is by the removal of some Mn^{2+} ions (half the concentration of

pyrH$^+$) from the $MnPS_3$ lattice during intercalation, thereby creating cation vacancies and consequently maintaining charge neutrality. The Mn^{2+} ions removed from the lattice would probably be solvated. The mechanism is easily verifiable by examining the Mn stoichiometry in the intercalated compound or by detecting Mn in the supernatant pyridine liquid of the reaction. It had been initially assumed that the stoichiometry of $MnPS_3$ does not change during intercalation since the diffraction pattern was recovered on deintercalation. Pure $MnPS_3$ is highly stoichiometric.

A preliminary check for the loss of manganese was carried out by recording the EPR spectra of the supernatant pyridine liquid after completion of intercalation. EPR spectra showed the presence of a paramagnetic species with $g = 2.00$ comparable to Mn^{2+}. The starting pyridine was free of paramagnetic impurities. The Mn content in the supernatant liquid and the Mn stoichiometry in the solid intercalate were quantitatively estimated (details given in the Experimental Section). The two estimates were in agreement within experimental error. The Mn deficiency was found to be 0.08 mol of Mn per mol of $MnPS_3$. By combining these results with the TGA and TPDS results, the true stoichiometry of the intercalated compound may be obtained. The stoichiometry is $Mn_{0.92}PS_3(pyrH^+)_{0.16}(pyr)_{0.39}$ for the 5.9-Å phase. The result of the CHN analysis (see the Experimental Section) tallies with that predicted for this stoichiometry. It may be recalled that there was an apparent discrepancy between the results of the CHN and TG analysis.

The origin of the proton is probably from trace amounts of H_2O present in the starting pyridine and it is unlikely to be from bipyridyl formation. This was confirmed by the observation that intercalation of rigorously dried pyridine was extremely difficut. The overall reaction scheme may hence be written as

$$2x\,\text{pyr} + 2x\,H_2O \rightleftharpoons 2x\,\text{pyrH}^+ + 2x\,OH^-$$

$$MnPS_3 + 2x\,\text{pyrH}^+ + y\,\text{pyr} + 2x\,OH^- \rightarrow (Mn_{1-x}PS_3)^{2x-}(\text{pyrH}^+)_{2x}(\text{pyr})_y + x\,Mn^{2+}(OH)_2^-(\text{in solution})$$

On exposure to the atmosphere, the neutral pyridine molecules in the solvation shell could exchange with water molecules to give the 3.4-Å phase, which shows a two-step weight loss in the TG.

$$Mn_{1-x}PS_3(\text{pyrH}^+)_{2x}(\text{pyr})_y \xrightarrow{H_2O} Mn_{1-x}PS_3(\text{pyrH}^+)_{2x}(H_2O)_y$$

This would explain why the position of the pyridine bands of the 3.4-Å phase are similar to those of aqueous pyridine.

The nature of the host–guest interactions is electrostatic. The stability of the intercalated compound comes from the Coulombic interaction between the negatively charged $(Mn_{1-x}PS_3)^{2x-}$ polyanions and the positive pyridinium cations. The neutral pyridine molecules which solvate the pyridinium cation help in screening out the repulsive forces due to the remaining positively charged pyridinium cations. It is interesting to compare the above with the situation existing for pyridine intercalation in the transition metal dichalcogenides (see Introduction) wherein the host–guest interactions are between the negatively charged layers and solvated pyridinium ions. Ignoring the question of the source of protons for the formation of pyridinium ions as well as the mechanism for preserving charge neutrality, it may be seen that the intercalated species and the electrostatic nature of host–guest interactions are identical although the nature of the chemical bonding of the host in these two classes of compounds is quite different. The neutral pyridine molecules in the solvation shell are exchangeable by H_2O molecules, giving rise to the phase characterized by a lattice expansion of 3.4 Å. Why the presence of H_2O molecules in the solvation shell changes the orientation of pyridine molecules is not clear. This new orientation implies that it is the guest–guest interactions rather than the host–guest interactions which determine the orientation of the intercalated molecules. Further evidence for the importance of guest–guest interactions rather than the host–guest interactions in deciding the orientation comes from the fact that the pyridinium ions solvated by pyridine molecules adopt a similar orientation (**B** of Figure 3) in the pyridine intercalated transition metal dichalcogenides.

The above schemes explain most of the observed features of the intercalation of pyridine in $MnPS_3$. These obviously explain how charge neutrality is maintained. It is also possible to resolve the contradiction between the XRD of the deintercalated samples and the thermal deintercalation product spectra by the following reaction

$$Mn_{1-x}PS_3(\text{pyrH}^+)_{2x}(\text{pyr or } H_2O)_y \rightarrow (1-x)\,MnPS_3 + 2x\,\text{pyr} + y\,(\text{pyr or } H_2O) + x\,H_2S + \text{sulfur} + \text{phosphorus sulfides}$$

It may be seen that in the above deintercalation reaction stoichiometric $MnPS_3$ is recovered from both phases (although in smaller quantities) by the liberation of H_2S, sulfur, and phosphorus sulfides. This explains how the $MnPS_3$ diffraction pattern was recovered on deintercalation and at the same time the detection of sulfur and phosphorus compounds as deintercalation products. Thus, pyridine intercalation in $MnPS_3$ is not a true intercalation reaction but rather an ion-exchange/intercalation reaction similar to that observed for intercalation of organometallic cations.[17]

Although Mn^{2+} vacancies are produced on intercalation, the structural integrity of the host lattice is preserved—apart from the c-axis dilation. This is not surprising, since the transition metal thiophosphate structure is known to support a large number of metal vacancies, e.g. $In_{2/3}PS_3$[41] has a structure identical with that of $MnPS_3$, but with $^1/_3$ of the metal sites vacant. In the following sections we consider how the above intercalation reaction scheme can explain most of the experimental observation.

If pyridine intercalation were to proceed by the same mechanism in all three compounds $MnPS_3$, $FePS_3$, and $NiPS_3$, then the determining factor would be the energy required to remove a cation from the lattice. Part of this energy would be compensated by the solvation of the ion. All three compounds ($MnPS_3$, $FePS_3$, and $NiPS_3$) are ionic, with metal–ligand interactions of nearly the same strength. The major difference is in the crystal field stabilization energy (CFSE) of the three ions. The CFSE for the three ions Ni^{2+}, Fe^{2+}, and Mn^{2+} are 12, 4, and 0 Dq, respectively, which would explain the observed ease of intercalation. A similar rationale had been established for the intercalation of organometallics in these compounds.[42]

The electrical conductivity and the optical and EPR spectra of the intercalated compound, $Mn_{1-x}PS_3(\text{pyrH}^+)_{2x}(\text{pyr})_y$, are identical with those of pure $MnPS_3$. Since charge neutrality is maintained by creation of Mn^{2+} vacancies in the lattice, the oxidation state of manganese remains unchanged, which explains the above observations.

A reason similar to the above holds for the gross similarities in the lattice vibrations of the pure and the intercalated compound. The creation of vacancies would, however, cause the distortion of the neighboring octahedra, which explain why the center of inversion of the lattice is lost and Raman active modes are observed in the IR spectra. Since the Raman modes are observed in the IR spectra, it appears that the effect of the vacancies is global rather than being localized. The effect, however, must be small since it is not observable in the XRD (Figure 3).

The two features manifested in the magnetic properties are (a) the lowering of the critical temperature as compared to the host material and (b) the isotropic weak ferromagnetism at low temperature. The lowering of the critical temperature (from 78 to 60 K) is due to a "dilution effect" because of the creation of vacancies.

The IR and Raman spectra of the pyridine-intercalated $MnPS_3$ samples show that the structure no longer possesses a center of inversion. This implies that the DM interactions may now be operative so that a weakly ferromagnetic canted state can be realized. As mentioned earlier, the fact that for the intercalated samples, both $\chi_\parallel$ and $\chi_\perp$ increases near T_N implies that the spins

(41) Soled, S.; Wold, A. *Mater. Res. Bull.* **1976**, *11*, 657–662.
(42) Clement, R.; Garnier, O.; Jegoudez, J. *Inorg. Chem.* **1986**, *25*, 1404–1409.

in different sublattices have different canting angles. Since pyridine intercalation proceeds with loss of some Mn^{2+} ions from the host lattice, it is possible that the spins of the Mn^{2+} ions neighboring these vacancies may show a different canting angle (either due to the single ion anisotropy DS_z^2 or antisymmetric exchange $d_{ij}S_i \times S_j$) from those ions which are further away from the defect. This may be a possible mechanism for the observation of nearly isotropic weak ferromagnetism. This was confirmed by the angular and temperature variation of the EPR spectra of single crystals of pyridine-intercalated $MnPS_3$ which will be published later.[33]

In hindsight, it is not surprising why the intercalation of pyridine in $MnPS_3$ and the transition metal dichalcogenides proceeds by such different mechanisms. The MPS_3 (M = Mn, Fe, Ni, etc.) are ionic and are best viewed as salts of the thiophosphate anion with the metal-sulfur bond length being reasonably approximated by the sum of the ionic radii.[7] The "d bands" are narrow and the materials are Mott insulators. In contrast, the transition metal dichalcogenides like TaS_2 are more covalent with d electrons delocalized, and the d band widths are large and consequently can easily accommodate an extra electron from the guest species. In $MnPS_3$, however, this would lead to highly localized electron densities (Mn^{1+}) at some centers. Since the Mn^{1+} state is unstable, the above mechanism is unlikely. On the other hand, $MnPS_3$ being ionic, the Mn-S linkages are weak so that the lattice energy required for the removal of a Mn^{2+} ion during an ion exchange is easily compensated by the electrostatic host-guest interactions as well as the solvation energy of the exchanged Mn^{2+} ion.

Metal-Induced Valence Isomerizations: Gas-Phase Reactions of Iron(I) and Copper(I) with Quadricyclane and Norbornadiene

Denise K. MacMillan, Roger N. Hayes, David A. Peake, and Michael L. Gross*

Contribution from the Midwest Center for Mass Spectrometry, Department of Chemistry, University of Nebraska—Lincoln, Lincoln, Nebraska 68588-0304. *Received July 8, 1991*

Abstract: Metal-promoted valence isomerizations and cycloreversions occur in the gas phase for adducts of norbornadiene (NBD) and quadricyclane (Q) with either Fe(I) or Cu(I). The collisionally activated decomposition (CAD) spectra of the adducts of NBD and Q with each metal indicate that the complexes possess identical structures, although the structures that are formed with Fe(I) are different from those with Cu(I). Both Cu(I) and Fe(I) cause the valence isomerization of Q to NBD. The metal ion then induces a retro Diels-Alder reaction of NBD to form a $(C_5H_6)M^+(C_2H_2)$ complex. Only the Fe(I) complexes react further to generate a $(C_5H_5)(H)Fe^+(C_2H_2)$ species. Structures of the adducts of toluene (T) and cycloheptatriene (CHT) with each metal are shown to be similar but non-interconverting with those of NBD and Q. Fourier transform mass spectrometry (FTMS) data provide additional support for the structural assignments. Experimental rate constants for the reactions are nearly equal to each other and to the collision rate constants for each system.

Introduction

The subject of gas-phase transition metal ion reactions with organic molecules has been a focus of numerous investigations in recent years.[1] Metal ion bonding energetics are one area of intense study;[2] however, much of the current effort in the field is concerned with the clarification of mechanisms of reactions such as oxidative addition and remote functionalization.[3] Some evidence for metal ion-induced retro Diels-Alder reactions[4] and other interesting condensations[5] was also revealed by mechanism studies. Little work, however, has been done with gas-phase metal-promoted isomerizations.[6]

There are, to our knowledge, no reported efforts to understand metal-ion-induced valence isomerizations in the gas phase although there are some examples reported for two-phase and condensed-phase systems. Hamilton et al.[7] reported the valence rearrangement of gas-phase Binor-S, a norbornadiene dimer, on a solid platinum surface. Greenberg and Leibman[8] as well as Bishop[9] provide numerous examples of the ability of transition metals in solution either to induce valence isomerizations of kinetically stable strained cyclic molecules or to stabilize transitory species.

We present in this paper the results of an inquiry into the ability of Fe^+ and Cu^+ to initiate valence isomerizations of quadricyclane[10] (Q) and norbornadiene[11] (NBD) in the gas phase. Both are strained C_7H_8 isomers and have been considered for possible chemical energy storage systems.[12] Isomerization of NBD to Q stores energy in Q. That energy is released upon reversion of Q to NBD.

Scheme I

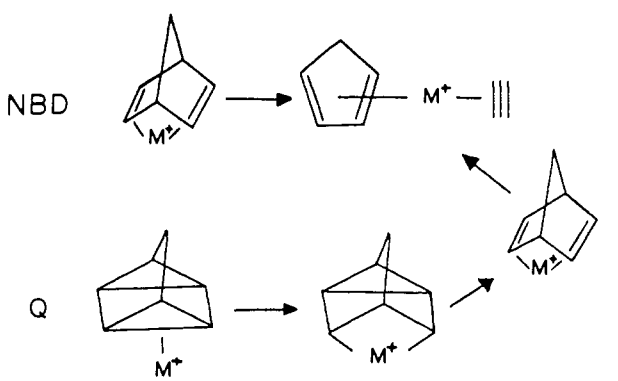

M = Cu, Fe

We used two complementary tools to study Fe^+ and Cu^+ adducts of C_7H_8 isomers: tandem mass spectrometry (MS/MS)

* Author to whom correspondence should be addressed.

(1) (a) *Gas Phase Inorganic Chemistry*; Russell, D. H., Ed.; Plenum Publishing: New York, 1989. (b) Schwarz, H. *Acc. Chem. Res.* **1989**, *22*, 282. (c) Armentrout, P. B.; Beauchamp, J. L. *Acc. Chem. Res.* **1989**, *22*, 315. (d) Squires, R. R. *Chem. Rev.* **1987**, *87*, 623. (e) Allison, J. In *Progress in Inorganic Chemistry*; Lippard, S. J., Ed.; John Wiley and Sons: New York, 1986; Vol. 34, p 627. (f) Freiser, B. S. *Talanta* **1985**, *32*, 697.

0002-7863/92/1514-7801$03.00/0